GEOPHYSICAL & ASTROPHYSICAL FLUID DYNAMICS, 2016
http://dx.doi.org/10.1080/03091929.2016.1164148

Taylor & Francis
Taylor & Francis Group

Interaction between a surface jet and subsurface vortices in a three-layer quasi-geostrophic model

M. A. Sokolovskiy[a,c], X. J. Carton[b], B. N. Filyushkin[c] and O. I. Yakovenko[c]

[a]Institute of Water Problems of RAS, Moscow, Russia; [b]Laboratoire de Physique des Océans, UFR Sciences, UBO, Brest, France; [c]P.P. Shirshov Institute of Oceanology of RAS, Moscow, Russia

ABSTRACT

This study focuses on the interaction between mid depth vortices and surface jets and fronts in a three-layer quasi-geostrophic model. Such vortices may be regarded as an idealisation of meddies, eddies of Mediterranean Water in the Northeastern Atlantic Ocean, interacting with the Azores j t and front. Successively, a single vortex, a vortex doublet and a vortex pair (in the middle layer) are studied. When a single vortex is considered, the jet has a critical effect of its motion, temporarily slowing down its zonal drift and accelerating it meridionally as the vortex crosses the front. On the contrary, if the vortex does not cross the front, it can drift fairly rapidly along it. The merger of a vortex doublet (two like-signed vortices) below a surface jet is possible whatever the relative position of this doublet with respect to the jet axis. Nevertheless, doublets initially located below the front, will undergo stronger shear and merger efficiency will be diminished. The merged vortex will be circled at the surface by a large meander of the jet. Finally, eastward jet-dipole interaction experiments are performed with various orientations of the vortex dipoles. Eastward propagating dipoles below the jet follow it without deformation. Southeastward drifting dipoles finally join the previous evolution. Southward and southwestward directed dipoles cross the surface jet southeastward. The presence of meanders initially on the jet does not prevent its crossing by a single vortex. Characteristics of the surface jet meanders are also described for a possible remote detection of this process.

ARTICLE HISTORY
Received 7 January 2016
Accepted 7 March 2016

KEYWORDS
Intrathermocline lens; meddy; dipoles; surface jet current; vortex-jet interaction; three-layer model

1. Introduction

1.1. Intrathermocline lenses formed from marginal sea outflows in several ocean basins

Marginal seas are semi-enclosed seas communicating with a neighbouring ocean, via a strait. These water areas can form salty waters due to an excess of evaporation; such waters are then exported into the adjacent ocean, under the form of a continental slope current. Such outflow currents can undergo instabilities, often triggered by topography anomalies on the continental slope; these instabilities can yield eddies. Since these outflow currents

CONTACT M. A. Sokolovskiy sokolovskiy@iwp.ru

stabilise hydrostatically at the thermocline level, the eddies thus formed lie at the same depth. These eddies are called intrathermocline eddies or intrathermocline lenses (ITLs).

For example, the Mediterranean Sea, the Red Sea and the Persian Gulf produce salty water masses by evaporation (respectively the Mediterranean Sea Water, the Red Sea Water and the Persian Gulf Water). These water masses are exported through the Strait of Gibraltar into the North Atlantic Ocean, or through the straits of Bab el Mandeb or of Hormuz, into the Indian Ocean. Once in these oceans, these three outflows stabilise respectively at 600–1600, 600–1000 or 200–350 m depths. The ITLs formed by the instability of these outflows can be cyclonic or anticyclonic vortices, though more of the latter have been observed (see below). Horizontally, they can have a quasi-circular or an elliptical shape (Armi and Zenk 1984, Filyushkin 1989, Prater and Sanford 1994, Käse and Zenk 1996).

In the North Atlantic Ocean, the warm and salty Mediterranean Water (MW) outflow is a major source of lens formation at depth ranging from 600 to 1600 m (Madelain 1970). The canyons in the Gulf of Cádiz are a well known area of MW lens formation (Ambar 1983, Armi and Zenk 1984, Aleynik *et al.* 1998, Johnson *et al.* 2002, Alvez *et al.* 2011); other generation areas are Cape St. Vincent (Bower *et al.* 2002), canyons of the western and northern shelves of Portugal and Spain (Richardson *et al.* 1989, Paillet *et al.* 2002) and the Gorringe Bank at the mouth of the Gulf of Cádiz (Serra *et al.* 2005). At these locations, the MW undercurrents generate single anticyclonic ITLs or dipolar ITLs (cyclone-anticyclone pairs). Dipolar ITLs also form from the penetration of a MW jet into the open ocean, south-west from Cape St. Vincent (Fedorov and Ginzburg 1989, Filyushkin and Plakhin 1996).

Anticyclonic MW lenses (meddies) are long lived: their average life time ranges from 1 to 4 years); thus, they can drift far away from the Iberian Peninsula where they are formed; they can be found from 20°N up to 48°N and from the Iberian Peninsula to 40°W (Armi and Stommel 1983, Richardson *et al.* 1989). On the contrary, cyclonic MW eddies tend to disappear rapidly away from the formation areas (their lifetime is usually shorter than a year). Via diffusion, both MW cyclones and anticyclones feed the MW "tongue" at 1000 m depth, which extends southwestward from the Strait of Gibraltar, over 3000 km.

MW lenses (both cyclonic and anticyclonic) are easily detected in situ, via CTD soundings; indeed, their high temperature and salinity anomalies with respect to the surrounding water masses, play the role of "natural tracers" (Thorpe 1998). MW lenses can be tracked in time using drifters with neutral buoyancy (Richardson *et al.* 1989, Carton *et al.* 2002, 2010, Filyushkin *et al.* 2014) or via their signature at the surface of the ocean: (Stammer *et al.* 1991, Pingree and Le Cann 1993a,b, Pingree 1995, Stammer 1998, Carton *et al.* 2010, Filyushkin and Sokolovskiy 2011, Bashmachnikov and Carton 2012, Bashmachnikov *et al.* 2014, Bashmachnikov *et al.* 2015, Ciani *et al.* 2015).

Hydrological databases, and regional models of the North Atlantic Ocean, provide the spatial distribution of Meddies (Käse and Zenk 1987, Kostianoy and Belkin 1989, Richardson *et al.* 1991, Richardson *et al.* 2000, Filyushkin *et al.* 2009, Aguiar *et al.* 2013, Bashmachnikov *et al.* 2015). The role of meddies in the heat and salt transport can be assessed knowing the annual rate of meddy formation (and their typical size). Serra *et al.* (2005) and Filyushkin and Sokolovskiy (2011) estimate that 25–30 meddies form per year with horizontal radii ranging between 20 and 50 km, and vertical thicknesses between 600 and 1000 m. Using an average horizontal radius is of 35 km and vertical thickness is 800 m,

meddies would contribute a flux of 2.7 Sv offshore (this represents about 70–80% of the total flux of MW at Cape St Vincent).

ITls also form from other marginal outflows: the Red Sea outflow Water (RSW) forms a salty tongue at 400–1000 m depths in the Gulf of Aden and in the Northwestern Indian Ocean. ITLs can detach from this tongue; these lenses play an important role in RSW advection (Fedorov and Meshchanov 1988, Meschanov and Shapiro 1998, Bower and Furey 2012). ITLs were also found to form from the destabilisation of the Persian Gulf outflow by surface mesoscale vortices (L'Hégaret *et al.* 2015, Vic *et al.* 2015). These lenses lie at a 200–350 m depth.

1.2. Observations of other ITLs in the World Ocean

ITLs with anomalous waters, not originating from marginal sea outflows, have been sampled in different ocean basins. For instance, ITLs can form from current meandering in the deep ocean, or close to coasts, and then drift over large distances.

In the North Atlantic Ocean, an ITL observed off the Bahamas in 1976 (McDowell and Rossby 1978) was found to have formed in the northwest corner of the North Atlantic Current (Prater and Rossby 1999). In the Sargasso Sea, many ITLs were observed at depths of 550 to 800 m (Dugan *et al.* 1982). In the same region, Brundage and Dugan (1986) have observed an anticyclonic vortex with temperature of water of 18°. In the Iceland Basin, ITLs with strong anticyclonic circulation and cold surface temperature anomaly were observed by Martin *et al.* (1998). Two different types of deep coherent eddies were detected during a mooring in the Labrador Sea (Lilly and Rhines 2002).

The "Megapoligon-87" experiment found a submesoscale eddy with a cold core south of the North Pacific Subarctic Front (Maximenko and Yamagata 1995). Subthermocline, lenslike anticyclonic eddies have been observed to form from the California Undercurrent (Pelland *et al.* 2013). In the South Pacific, a few lenses were found at 100–350 m depths, and their interaction with a complicated relief of the Juan Fernández Archipelago has been investigated (Andrade *et al.* 2014). In the Tasman Sea, lenses of 40 km in diameter and thickness of 200–300 m were observed in the centre of three large anticyclonic eddies due to he sinking of dense continental shelf water (Baird and Ridgway 2012). ITLs with a 100 km diameter and a thickness larger than 100 m were observed near the Tsushima Current in the Japan Sea (Gordon *et al.* 2002, Hogan and Hurlburt 2006). Subsurface cyclonic and anticyclonic eddies have been found in the Arctic Ocean at depths between 50 and 300 m (Hunkins 1974).

Belkin *et al.* (1986) pointed out the important role of lenses in the transport of intermediate waters. In the course of their drift, lenses can be affected by the bottom relief, by the continental shelf, by surface jets or fronts or by other vortices or lenses (Baird and Ridgway 2012, Sokolovskiy *et al.* 2013, Sokolovskiy and Filyushkin 2015). Indeed, ocean models and observations have shown that several lenses can coexist locally and thus interact (Schultz Tokos *et al.* 1994, Bower *et al.* 2002, Serra *et al.* 2010, Aguiar *et al.* 2013, L'Hégaret *et al.* 2014). The interaction between lenses, and with a surface jet, is therefore of interest.

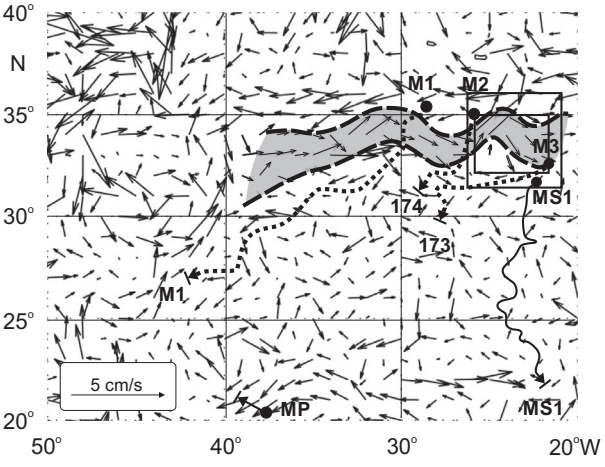

Figure 1. Currents in the area in the NW Atlantic at the depth of 1000 m, based on ARGO float data, averaged over 2004–2015 (Lebedev 2016). The grey area represents a fragment of the AFZ, and the dashed lines show its boundaries. The dotted line shows the trajectories of lenses M1 (SEMAPHORE) (Richardson and Tychensky 1998) over a period of 533 days, and solid line shows MS1 (SHARON) (Armi *et al.* 1989) over a period of 2 years. The another dotted lines show the trajectories of lenses M2 over 200 days and M3 over 333 days, and the positions of buoys 174 and 173 show the sites of their destruction (Richardson and Tychensky 1998). The round markers shows the initial positions of lenses and the arrow with a terminator shows their final coordinates. MP is the position of the MESOPOLYGON lens on June 26, 1985, at the point with coordinates (20°N; 37°W) (Ivanov *et al.* 1998). The large square area in the top right part of the figure embraces the zone of SEMAPHORE experiment, and the smaller domain is the area of the hydrological survey of R/V "Professor Shtokman" (Ivanov and Filyushkin 1995).

1.3. Azores jet – meddy interaction

In the course of their southwestward drift, Mediterranean ITLs often cross the Azores Frontal Zone (AFZ) and the Azores Current. The Azores Current is associated with subtropical convergence. Surface drifter tracking often locate this current near 34°N (Zhou *et al.* 2000). The Azores Current is also identified between 0 and 1000 m depths, by analysing ARGO float observations (Lebedev 2016, see also http://argo.ocean.ru). In situ data and satellite observations show the frequent presence of meanders on the Azores Current, with width up to 130 km, and velocities of 9–14 cm/s at the surface, 2–6 cm/s at 600 m depth, and 1–2 cm/s at 1000 m (Käse and Siedler 1982, Ivanov and Filyushkin 1995).

The main studies of the interaction between Mediterranean ITLs and the jet Azores Current were carried out during the SEMAPHORE experiment (July 1993 – January 1995) (Richardson and Tychensky 1998, Tychensky and Carton 1998). The study area was bounded by latitudes 31.5–36.0°N and longitudes 20.5–26.0°W. It was crossed by the Azores Current. Four MW lenses were identified in the area (figure 1). Figure 1 shows the currents at 1000 m depth, averaged over 10 years of ARGO float observations (2004–2015), and the initial and final positions of 3 lenses identified and followed during the SEMAPHORE experiment.

Lens M1, detected in July 1993, was located 200 km west of the test area and north of the AFZ, moving southwestward. It lay at depths of 650–1500 m. By late October, it crossed the frontal zone nearly meridionally without performing loops (Richardson and Tychensky 1998, figure 4), and then drifted southwestward until its destruction in January 1995. This

trajectory of lens M1 near the Azores Current could be due in part to the influence of seamounts west of its position. The velocity of the Azores current at 1000 m depth was then 1–2 cm/s, and the drift velocity of M1 about 3.9 cm/s. This large MW lens (120 km in diameter) had two cores showing anomalous temperature and salinity at depths of 850 and 1250 m. Another large lens, M3, 150 km in diameter, was detected in October 1993 from R/V "Professor Shtokman" (Ivanov and Filyushkin 1995) south of the Azores Current. In November 1993, buoy 173 was introduced into this lens (Richardson and Tychensky 1998). This lens also had two cores vertically (at 900 and 1200 m) (Richardson and Tychensky 1998, figure 4). The presence of very large MW lenses near the Azores Current can support the hypothesis of MW lens merger in the AFZ zone. Lenses M2 and M3 directly interacted with the jet current: M2 crossed it, while M3, coupled with a meander; this coupling then yielded a complex structure comprised of a cyclone and of fragments of the lens (Richardson and Tychensky 1998, figure 2).

Observations of lenses in this area suggest that

(1) Meddies can be found on both sides of the AFZ. They drift from the north, cross the Azores current, and keep drifting until complete destruction (figure 1, lenses Sharon 1, SEMAPHORE 1). Therefore, we can regard AFZ as partially transparent for the passage of lenses.
(2) Conditions for the formation of large lenses can be met near the front: when several lenses are present north of the front, they can interact or merge (if two lenses come closer to one another, than a critical distance) (Filyushkin and Sokolovskiy 2011). Large lenses can result from mutual lens interaction or interaction with the jet: in figure 1, these are M1 (SEMAPHORE), MS1 (SHARON), MP (MESOPOLYGON).

Unfortunately, the limited spatio-temporal extent of observations (especially in 4D) does not allow a thorough analysis of Azores Current-multiple ITL interactions. Therefore, we resort here to numerical simulations to analyse various scenarios of interaction between the lenses and the frontal jet.

2. Model

For simplicity, but keeping realism, we will use a three-layer quasi-geostrophic model with parameters characteristic of the North Atlantic Ocean at mid latitudes: the depth is 4 km, thicknesses of the upper, middle and bottom layers are $h_1 = 600$ m, $h_2 = 1000$ m and $h_3 = 2400$ m correspondingly, and the first and second radii of deformation are $Rd_1 = 32$ km and $Rd_2 = 15$ km (Sokolovskiy *et al.* 2013).

In this model, we idealise the intrathermocline vortex (cyclone and anticyclone) as a vortex patch with constant positive or negative values of PV, correspondingly, located in the intermediate layer.

We set a length scale R^* equal to $Rd_1 = 32$ km, a time scale T^* equal to a rotational period of an initially circular vortex patch of unit radius, in absence external field. So, if we assume the maximum velocity on the circular vortex contour of unit radius to be 40 cm/s, we obtain $T^* \approx 9$ days.

The equations governing potential vorticity (PV) in the three-layer quasi-geostrophic model on the f-plane are (Sokolovskiy and Verron 2014):

$$\frac{\mathrm{d}_j q_j}{\mathrm{d}t} = 0,$$

where $j = 1, 2, 3$ being the upper, middle and lower layer indices respectively, and

$$\begin{bmatrix} q_1 \\ q_2 \\ q_3 \end{bmatrix} = A \begin{bmatrix} \psi_1 \\ \psi_2 \\ \psi_3 \end{bmatrix}, \qquad A = \begin{bmatrix} \nabla^2 - \dfrac{F_1}{h_1} & \dfrac{F_1}{h_1} & 0 \\ \dfrac{F_1}{h_2} & \nabla^2 - \dfrac{F_1 + F_2}{h_2} & \dfrac{F_2}{h_2} \\ 0 & \dfrac{F_2}{h_3} & \nabla^2 - \dfrac{F_2}{h_3} \end{bmatrix}.$$

Here $\mathrm{d}_j/\mathrm{d}t = \partial/\partial t + u_j\partial/\partial x + v_j\partial/\partial y$ and $\nabla^2 = \partial^2/\partial x^2 + \partial^2/\partial y^2$ are the 2D–operator of total time derivative and Laplace operator, respectively; q_j, ψ_i and u_j, v_j are the PV, stream-function and horizontal components of velocity for the jth layer, $F_n = \rho_0 (fR)^2/(g\Delta\rho_n H)$; ρ_0 is the mean density value, f is the constant Coriolis parameter, g is gravity acceleration, $\Delta\rho_n = \rho_{n+1} - \rho_n$ $(n = 1, 2)$; ρ_j is the constant fluid density in the jth layer, $H = h(h_1 + h_2 + h_3)$ is the total depth, and h and R are the characteristic vertical and horizontal scales, such that $h_1 + h_2 + h_3 = 1$.

The Froude numbers F_1 and F_2 are connected with the eigenvalues λ_j of the stratification matrix (Sokolovskiy 1997a,b):

$$\lambda_1 = 0,$$
$$\lambda_{2,3} = \frac{1}{2}\left[\frac{F_1}{h_1} + \frac{F_1 + F_2}{h_2} + \frac{F_2}{h_3} \mp \sqrt{\left(\frac{F_1}{h_1} + \frac{F_1 + F_2}{h_2} + \frac{F_2}{h_3}\right)^2 - 4\frac{F_1 F_2}{h_1 h_2 h_3}}\right],$$

where $\lambda_{2,3} = \left(R/Rd_{1,2}\right)^2$.

3. Numerical experiments

In layer number j $(j = 1, 2, 3)$, PV is assumed to have a piecewise constant distribution $q_j = \sum_{i=1}^{N_j} q_{ij}$, where q_{ij} are constants inside compact domains with areas S_{ij} and are equal to zero outside (they are vortex patches). N_j is the number of vortex patches in the jth layer.

The numerical model is based on a three-layer modification of the Contour Dynamics Method (CDM) (Sokolovskiy 1991), with the procedure of Contour Surgery (CS) (Dritschel 1988, Makarov 1991). Each patch of uniform PV is bounded by a contour discretized with nodes. These nodes are advected by the flow generated by the PV patches. The CS cuts off long and thin vortex lines, and removes overlapping boundary segments when the vortex patches with the same PV approach one another (and even merge). The same procedure admits the mechanism of artificial "dissipation", ignoring the vortex structures whose contours contain nodes whose number K is less than some specified value K_{min}. This Lagrangian method is very convenient for studying the contour evolution of the vortex patches.

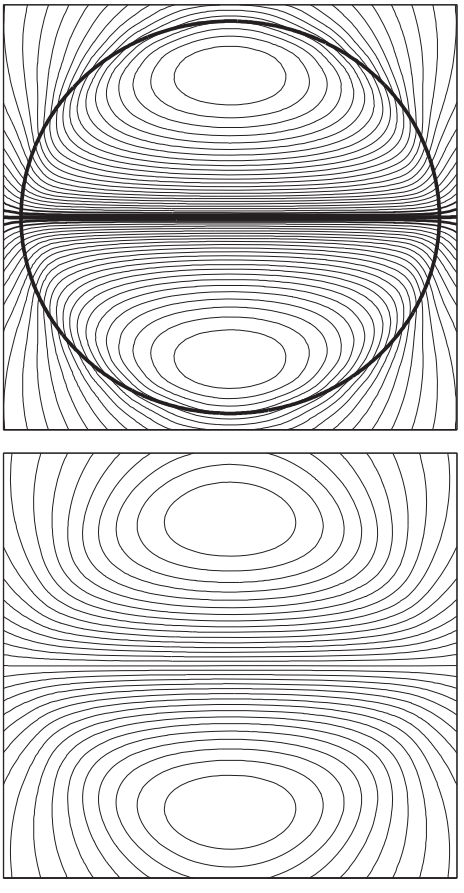

Figure 2. Top panel: the background state in the form of two surface semicircular gyres with cyclonic (northern) and anticyclonic (southern) motion. The boundaries of the gyres are given by thick lines. The thin lines show isolines of the stream–function for upper layer. The semithick lines are five isolines corresponding to maximal zonal velocities. Bottom panel: streamlines for middle layer of a three–layer fluid induced by the upper–layer flow.

In this section, we will examine different mutual interactions of lenses (vortex patches) and a large scale gyre using three-layer quasi-geostrophic CDM, and we will study the characteristics of their joint evolution.

3.1. Surface jet current

By surface jet (shear) flow, we mean a unidirectional flow along the interface between two semicircular gyres with opposite signs of rotation (Kozlov and Sal'nikov 1989, for example) confined to the top layer of the model three-layer ocean. Let us suppose that a cyclonic vortex lies in the upper part of the panel and an anticyclonic vortex, in its lower half; then a zonal jet current directed eastward will be initiated near the rectilinear segment of the boundaries of vortex patches. The contours of the vortex patches are given by thick lines in the top panel in figure 2.

The radius of the semicircular large-scale gyres is taken equal to $R = 12R_d = 384\,\text{km}$. The contact line in the middle of the domain is 768 km long. This corresponds to the axis of

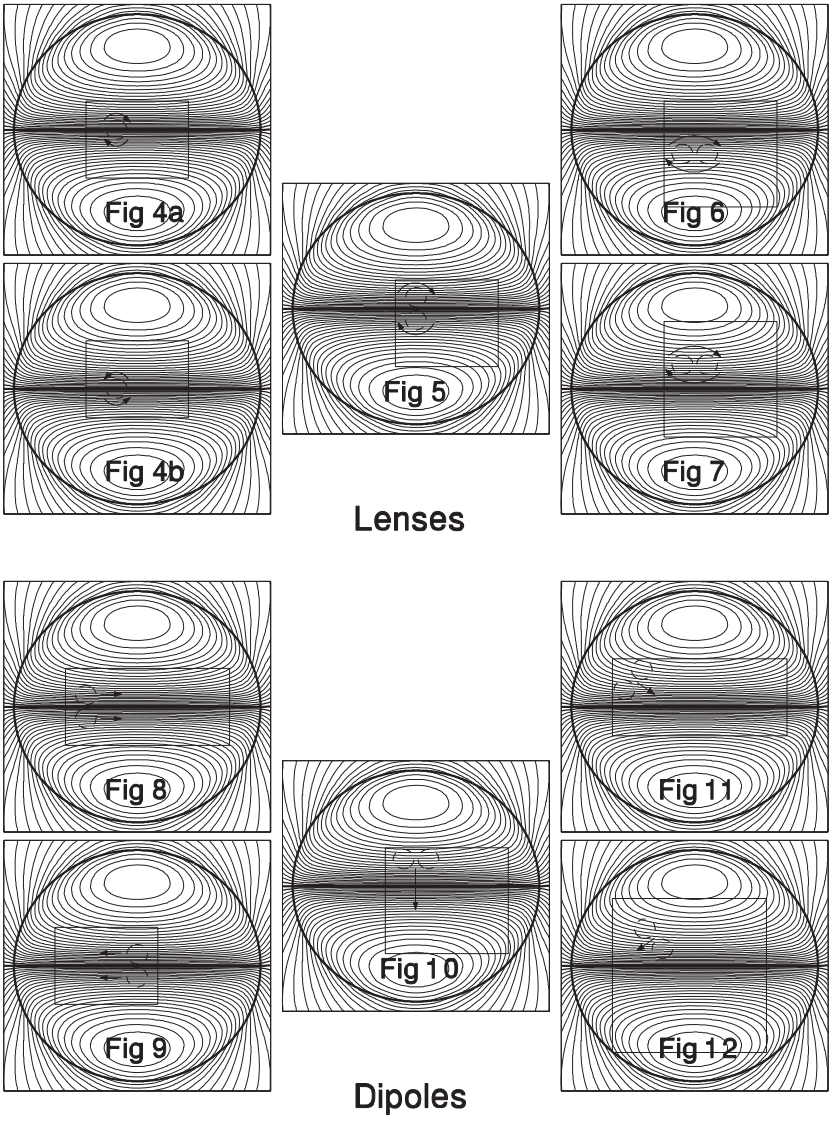

Figure 3. Gyres contours and streamlines in the top layer. The frames in each panel depict the domains where, in figures 4–12, the vortex-contour and streamline evolutions are shown. The dashed lines represent the manifestation of the middle-layer vortex contours in the upper layer. The arrows show the direction of rotation (or translational motion) of vortices (or pairs of vortices) in the middle layer.

the jet associated with a PV front, referred to as a dynamic or as a Lagrangian front (Prants *et al.* 2014). In the steady-state case, it coincides with the axis of the kinematic front, which is shown in the top panel of figure 2 as a bundle of semithick streamlines with maximal zonal velocities. The magnitude of potential vorticity P_g for the gyres is such that the velocity of fluid particles V_g on the external boundaries of gyres is 20 cm/s.unboundedresemble a Lamb vortex (Lamb 1932), or a Lamb–Chaplygin vortex (Kizner and Khvoles 2004), or a Lamb–Oseen vortex (Antkowiak and Brancher 2004, for example). Such dipolar vortices display self-translation. Therefore, the interaction of the jet with ITLs is studied in a co-moving coordinate system.

The (anticyclonic and cyclonic) ITLs will be initialised as circular vortex patches of uniform PV in the middle layer, with a radius R_m and potential vorticities $P_m = V_m(1 + R_m/R_d)/R_m = 2V_m/R_m$, assuming $R_m = R_d$ and $V_m = 2V_g$. Thus, the lenses are small and intense intrathermocline vortices. The lower layer will be considered as passive.

The numerical experiments, whose results are given in figures 4–12, show the details of jet-meddy/meddies interactions. Vortex patch contours and streamlines in the top and middle layers will be displayed in rectangular domains framed in figure 3.

3.2. Lenses and surface jet interaction

3.2.1. Intrathermocline vortex under a front (symmetric case)

Figure 4 shows the interaction of a single intrathermocline vortex in the middle layer, originally lying strictly under the front. Under the effect of the zonal flow, both cyclones and anticyclones first move eastward, and then, as they induce a deformation of the front, move meridionally. The ITL flow is clearly isolated in the middle layer streamlines, while their effect on the surface streamlines is initially much weaker. The surface signature of the ITL, observed by Bashmachnikov and Carton (2012), Bashmachnikov *et al.* (2014), Filyushkin *et al.* (2011), is smeared here by the intense surface current. An indirect signature of the presence of the ITL is manifested nevertheless by the clockwise wrapping of the jet meander around the position of the intrathermocline vortex. The front deformation increases with time, involving the growth of shorter wavelength components. The meander gives birth to a filament. The dynamical coupling of this filament with the ITL leads to the observed drift of the latter.

3.2.2. Two lenses below and near a surface jet

The following three experiments, illustrated in figures 5–7, show the behaviour of two intrathermocline anticyclonic vortices, lying close to each other (the distance between the centres of vortex patches of unit radius is 2.4). The vortices, rotating clockwise around a common vorticity centre, merge very quickly: at $T = 1$, i.e. after about 9 days, they approach one another still remaining separate vortices; however, as early as $T = 2$, they merge to form a single compact vortex (e.g. Filyushkin *et al.* 2010, Filyushkin and Sokolovskiy 2011).

The further evolution of the vortex in these three cases is somewhat different.

In figure 5, the intrathermocline vortices initially lie on opposite sides of the jet axis, but after time $T = 2$ they have already started merging. this indicates that their horizontal interaction is strong. Here, the unit ratio of vortex radius and deformation radius should render horizontal and vertical lens or jet interactions a priori similar for similar intensities and distances of flow components. But due to the strong intensity of the lenses, the intra-layer interaction is predominant here; the upper-layer front has little effect on the lens merging. As a result of merging of two lenses, a newly-formed larger vortex has completely moved into the anticyclonic gyre at time $T = 6$. It ejects filaments and small-scale vortices. With time, the small structures disappear, due the artificial dissipation caused by the contour surgery. By the end of the calculation period we observe only two anticyclones: a larger one and a smaller one, in co-rotation. They produce a deformation of the upper-layer jet, similarly to the smaller, single lens of figure 4(a). Nevertheless, this deformation

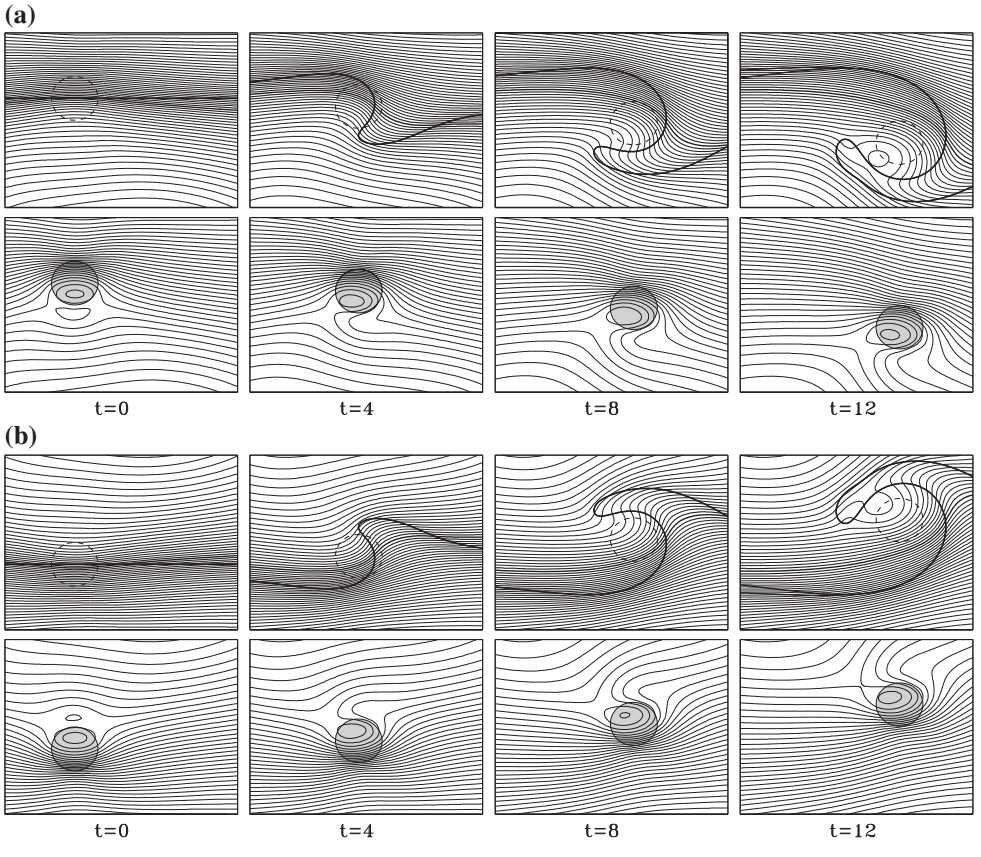

Figure 4. Interaction of a single intrathermocline vortex with a zonal jet current: (a) anticyclonic vortex (meddy); (b) cyclonic vortex. In both cases, the initial coordinates of vortex centre are (0; 0). The bottom panels show instantaneous configurations of vortices against the background of streamlines of the middle layer at the specified dimensionless times. In the top panels, the dashed lines recall the contours of intrathermocline vortices, the thick lines are the contours of surface gyres, the semithick lines show the kinematic front, and the thin lines are upper-layer streamlines at the same tames.

is more intense here and the upper-layer PV filaments are more stretched out by the larger and stronger ITL.

In figure 6, the lenses are originally located inside the southern gyre and they are initially parallel to the axis of the front. The merger of the original ITLs leads to a rotating configuration of three like signed vortices in the middle layer. Originally located farther from the surface front than the ITLs in the previous experiment, they are subject to a weaker shear. This weaker jet-vortex interaction is also apparent at the final stage of the experiment ($T = 12$): both the axes of the jet and the Lagrangian front show lesser deformations than those in figure 5.

Now the lenses are originally located under the northern cyclonic gyre (figure 7). The anticyclonic vortex and its small satellites, which have formed as the result of merging, move southeastward as a single structure, coupled with the surface jet meander. This meander displaces part of the anticyclonic large-scale gyre into the cyclonic one. The upper-layer kinematic front, locally driven southwestward by the middle layer lens, reflects the lens position at the ocean surface. In this latter case, the final (merged) vortex is still

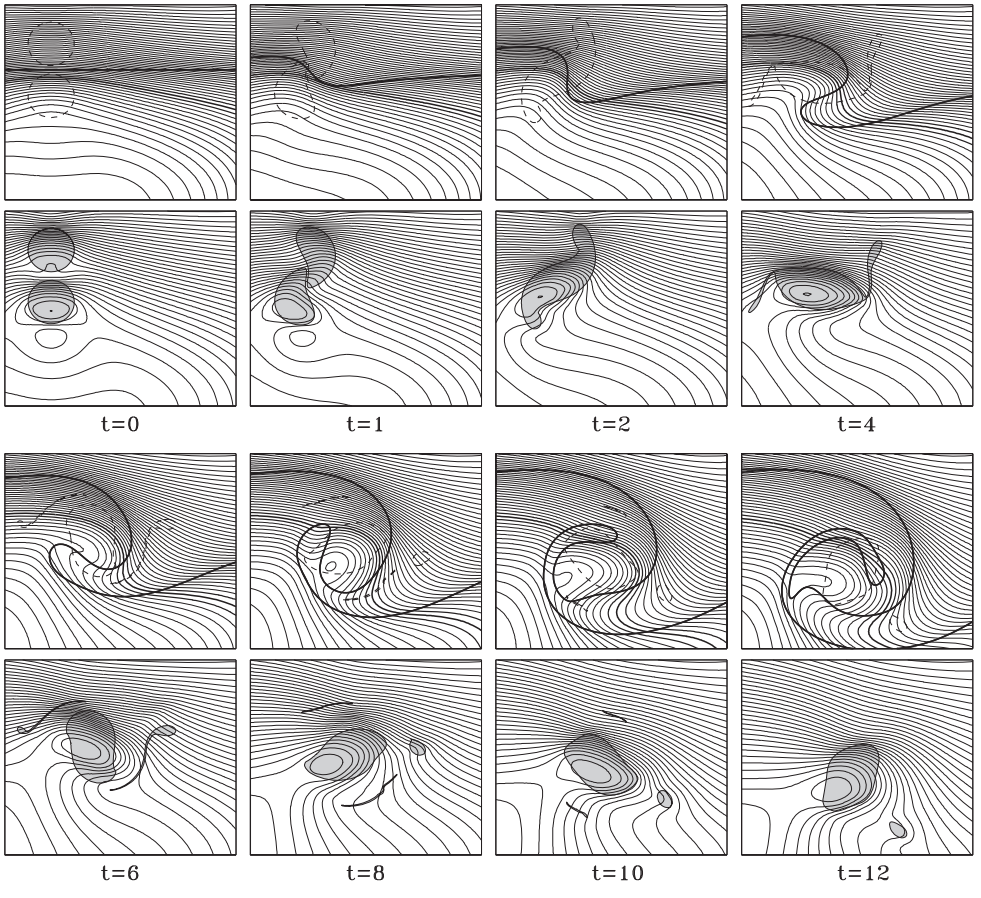

Figure 5. Same as in figure 4(a), but for two meddies initially centred at (0; ±1.2).

strongly deformed by the surface PV front at the end of the simulation. This may lead to further filamentation and weakening of this vortex at later times.

Note the intense *interaction* between the jet and the lens in all three experiments. On the one hand, the originally eastward flow in the top and middle layers considerably deviates southward. On the other hand, it thus forms an obstacle to the zonal drift of the lens.

3.3. Dipole of the middle layer in the neighbourhood of the surface jet

In this section, we study the interaction between the upper-layer jet and vortex pairs (meddy+cyclone) in the middle layer. Note that various problems of the dynamics of intrathermocline vortex pairs are discussed in Carton *et al.* (2002), Käse and Zenk (1996), Richardson *et al.* (2000), Sadoux *et al.* (1989), Serra and Ambar (2002), Serra *et al.* (2010).

3.3.1. A dipole moving parallel/antiparallel to the flow

A vortex pair travelling in the direction of the jet, or in the opposite direction, leads to very different responses of the flow.

Indeed, if both vortices of the pair are located under gyres with the same signs of potential vorticity (figure 8), the translation of the dipole takes place in the same direction

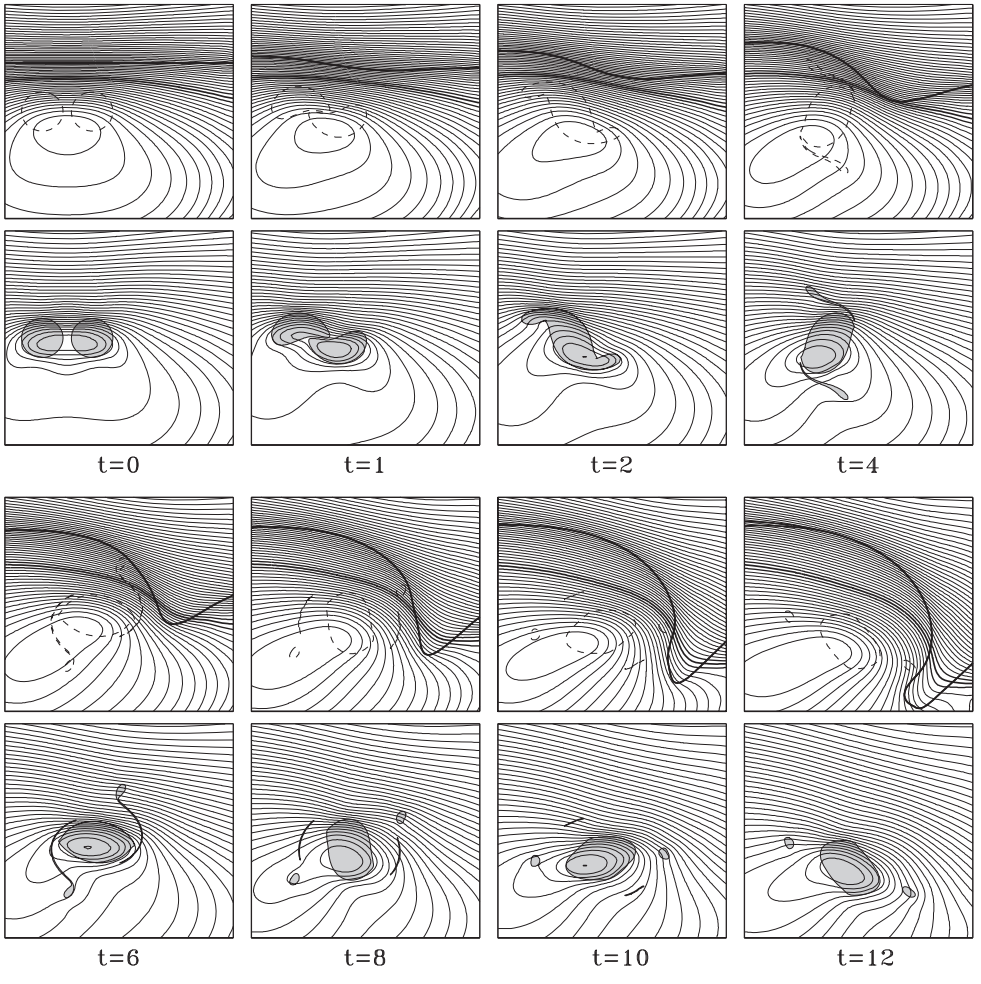

Figure 6. Same as in figure 5, but for two meddies initially centred at ($\pm$ 1.2; $-$2.5).

as the jet flow, and the vortex pair has almost no effect on the topology of the upper layer front, except for a local pincing of the streamlines, corresponding to an acceleration. In the middle layer, the flow between the vortex patches also intensifies.

The interaction of a dipole with an oppositely propagating jet is quite different (figure 9). Here, the velocity of the dipole is larger than that of the jet, so the dipole has a retrograde motion relative to the jet and this causes its swelling: the crests of the streamlines in the upper layer, move westward along with the vortex pair. The originally rectilinear front between the two gyres evolves as follows:

(i) the streamlines diverge upstream of the vortex pair and are "sucked" into the dipole domain downstream (this can be seen most clearly at $T = 12$);
(ii) the vortices of the pair "creep" into this swelled region between the gyres, and small U-shaped vortex patches detach from the downstream intrusions and move along the periphery of the middle-layer dipole.

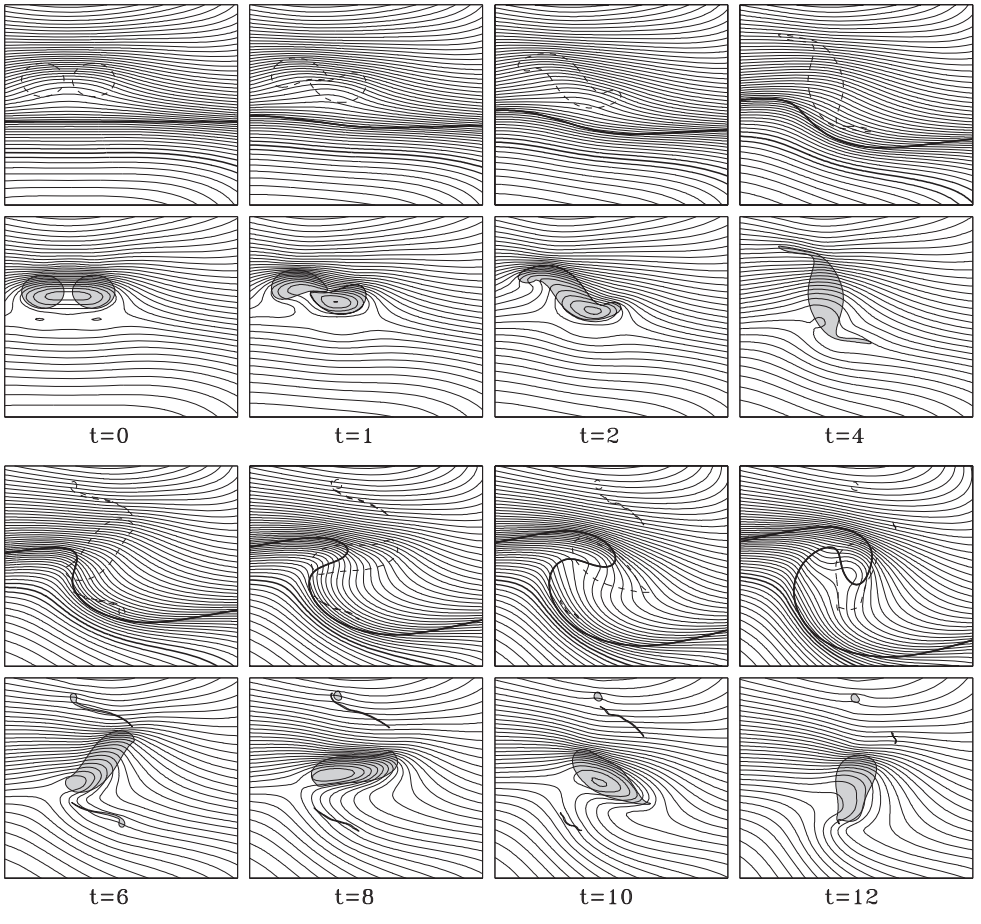

Figure 7. Same as in figure 6, but for two meddies initially centred at ($\pm$ 1.2; 2.5).

It is important to note that the translation velocity of the pair increases after it reaches the boundaries of gyres (compare for instance, the dipole displacement in intervals [0; 4] and [24; 28]). The eastward flow around the dipole is then almost the same as that in the steady-state case (Kizner and Khvoles 2004, figure 3(a)).

3.3.2. A dipole moving at an angle with respect to the flow

Figure 10 gives an example of the interaction between a surface jet and a pair of intrathermocline vortices, moving toward the jet at a right angle (270°). The dipole deforms the jet symmetrically and then the two vortices slowly diverge: the cyclone remains north of the surface PV front while the anticyclone crosses the front. Again, this front is strongly deformed by this interaction and takes the form of a mushroom vortex. The middle layer cyclone, coupling with the upper layer cyclonic meander advects the middle layer anticyclone anticlockwise. It must also be noticed that the upper layer front deforms and forms a cyclonic filament south of this anticyclone. Nevertheless, the coupling between this filament and the intrathermocline anticyclone is too weak to counteract the anticlockwise rotation.

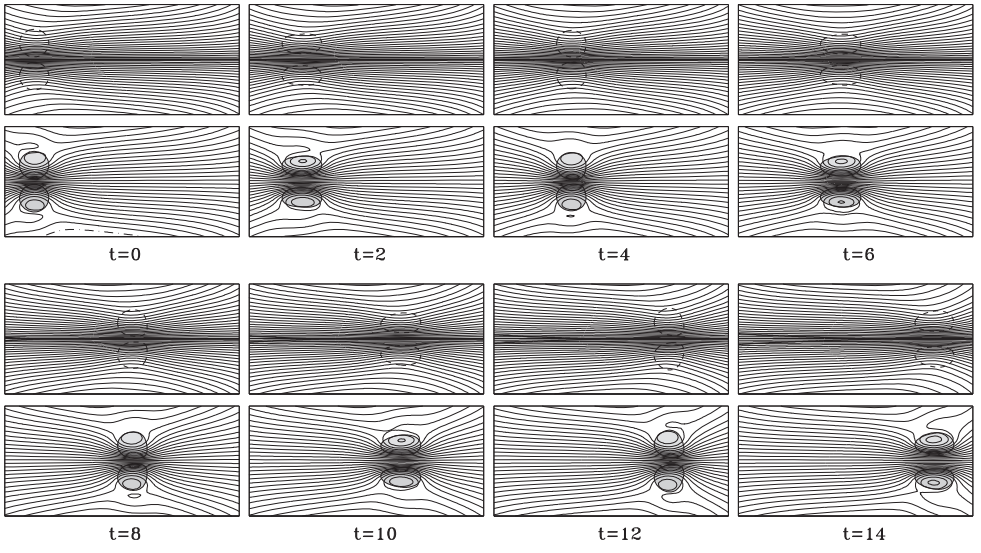

Figure 8. Vortex pair of the middle layer, moving along the surface jet and initially centred at $(-5; \pm 1.2)$.

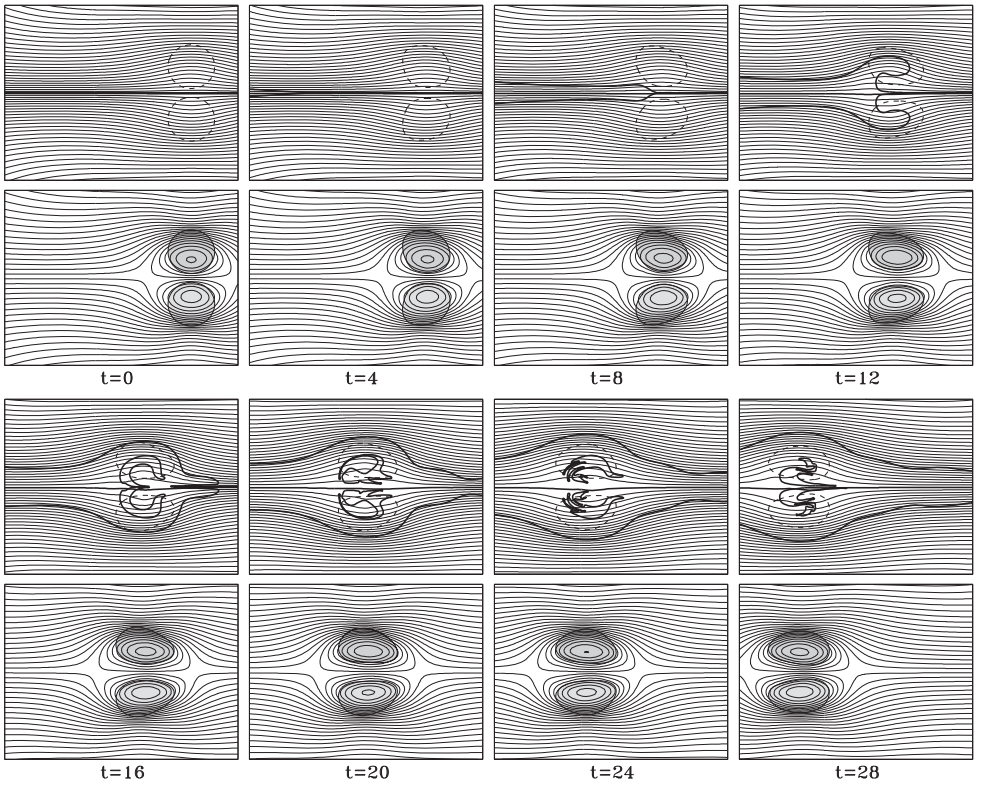

Figure 9. Vortex pair of the middle layer, moving against the jet surface and initially centred at $(0; \mp 1.2)$.

Figure 11 shows the interaction between a surface jet and a dipole in the middle layer, which starts at an angle of 315° with respect to the jet direction. Under the effect of the eastward jet, the angle of attack of such pair first decreases, reaching zero near $T = 12$, then

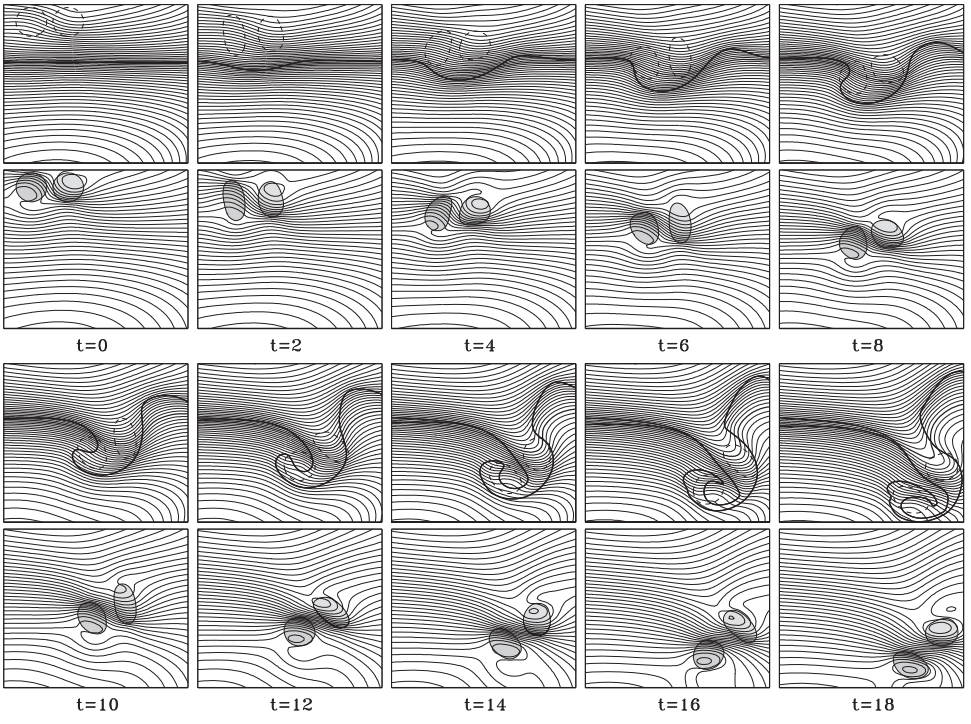

Figure 10. Vortex pair of the middle layer, moving perpendicular (at an angle of 270°) to the surface jet, and initially centred at ($\pm$1.2; 2.8).

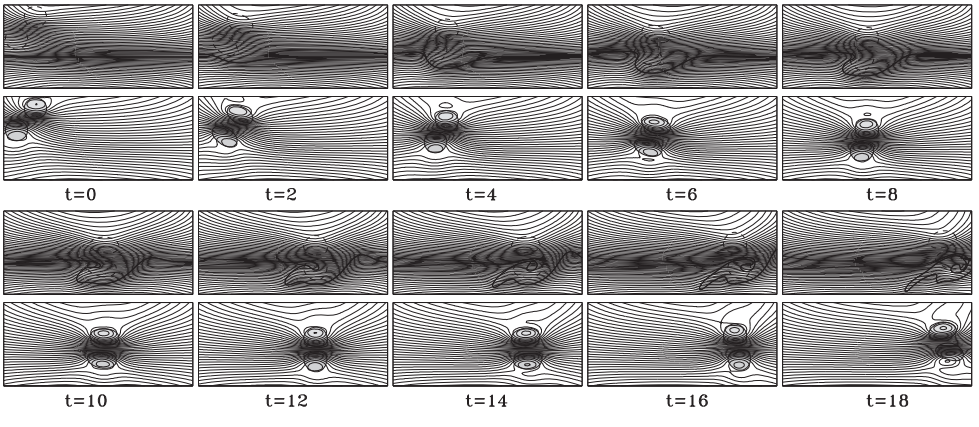

Figure 11. Vortex pair of the middle layer moving at an angle of 315° with respect to the surface jet and initially centred at (−6.8485; 1.7515) for the anticyclone and at (−5.1515; 3.8485) for the cyclone.

slightly changes sign. Thus, the dipole behaves as if it reflects on the jet. But essentially the dipole propagation is eastwards at late times. At the surface, the kinematic front remains weakly perturbed. A weak filament circles the southern anticyclone.

The experiment illustrated by figure 12 is devoted to the interaction between the surface jet and the intrathermocline pair running onto the flow at an angle of 225°, i.e. having

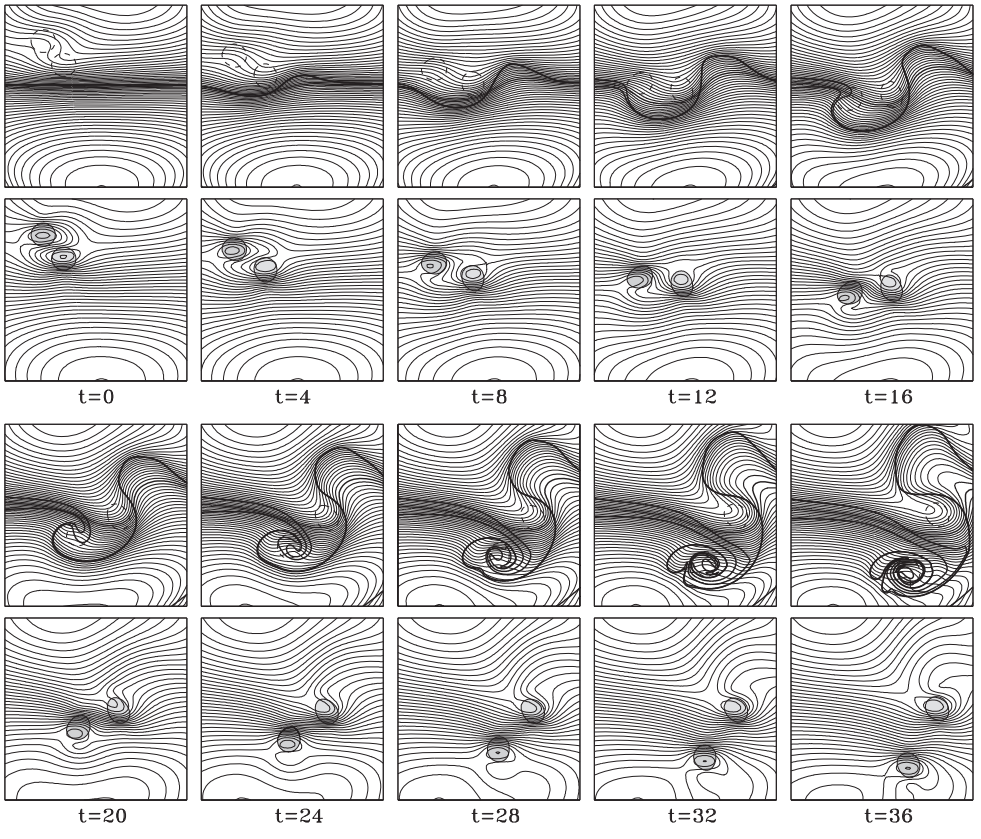

Figure 12. Vortex pair of the middle layer moving at an angle of 225° with respect to the surface jet and initially centred at (−3.1515; −1.7575) for the anticyclone and at (−4.8485; −3.8485) for the cyclone.

a component of motion against the flow. Such dipolar structure at the first stage rotates anticlockwise, during the period $T = [12;\ 16]$, the attack angle overshoots the value of 270° and finally becomes essentially eastward. The upper jet undergoes a deformation with positive and negative curvature (see again Appendix). As the upper jet and front deformation grows, they form short wavelength components corresponding again to filaments wrapping around the vortices, and forming a complex tangle, but with a global mushroom shape. This mushroom-shaped configuration has a characteristic horizontal scale exceeding the dimensions of intrathermocline vortices by a factor of 4–5.

Note again that the cyclonic vortex remains north of the deformed front, and that the dipole is slowly torn apart. Indeed, the souther n anticyclone now couples with a surface cyclonic filament and slowly drifts southward. A new (now baroclinic) dipole is formed.

In all examples of jet-dipole interaction considered above, the shape of vortex patches of the middle layer is barely changed at all times (they sometimes become elliptical). They are intense and have a size close to the radius of deformation R_d so that the shear flow across them is weak.

3.3.3. The case of a perturbed front

All cases studied above used an initially straight boundary between the gyres. Here we consider a more realistic case of an initially perturbed front – see figure 1. The gyre

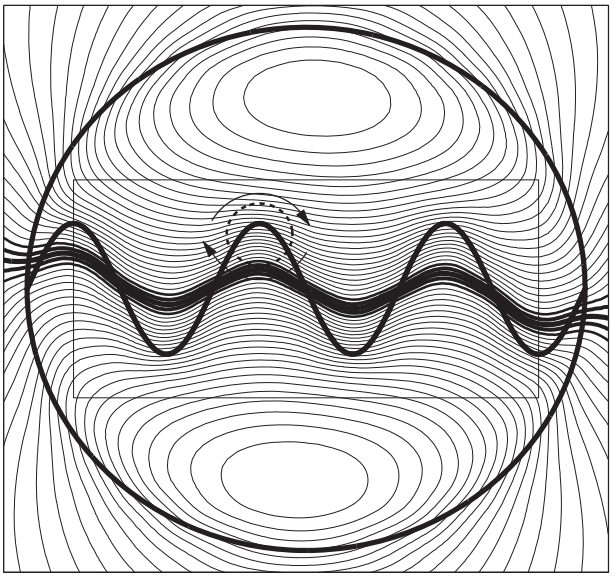

Figure 13. Contours of gyres (thick lines) at $A = 3$, $m = 3$, streamlines of the top layer (thin lines), and "reflection" of lens contour located in the middle layer (dashed line). The curved arrows show the direction of lens rotation. The rectangular frame shows the boundaries of the domain used to construct figure 14.

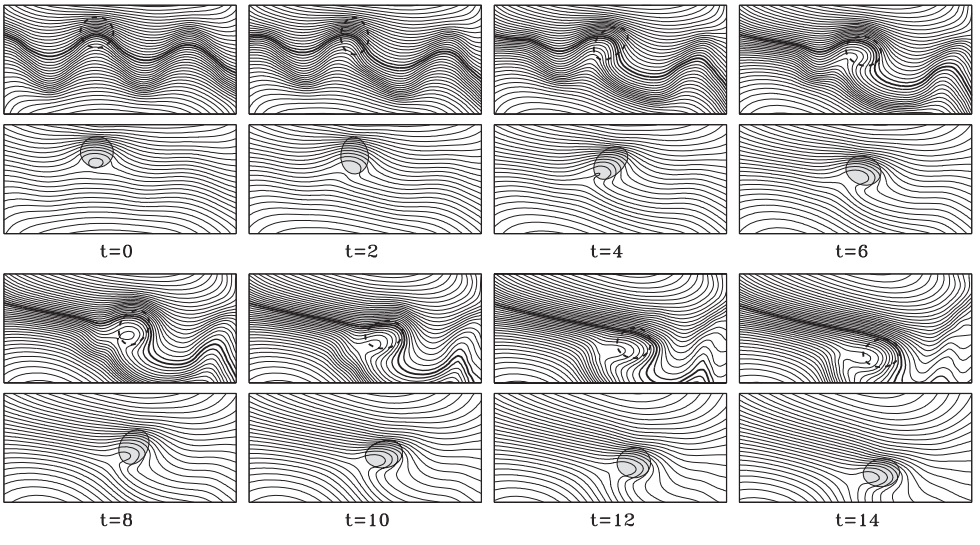

Figure 14. The motion of the lens with radius $\sqrt{2}$ initially located at $(-2; 2.5)$ in the flow field induced by a surface meandering front.

boundary is described by an equation of the type $y = -A\sin\left(m\pi x/R\right)$, $|x| \le R$, and the lens area is twice as large as before.

The parameters of this experiment were chosen to qualitatively reproduce the meanders of the Azores Current with an amplitude on the order of the lens radius; thus we aim to qualitatively reproduce the trajectory of "Meddy 2" (Richardson and Tychensky 1998, figure 2).

The lens centre (figure 13) is initially located between the loci of maximal deviations of the dynamic and kinematic fronts, i.e. it lies in the domain under the southern anticyclonic gyre, but north of the kinematic front.

Figure 14 shows the motion of such a lens under the effect of a meandering surface jet flow. The semithick lines on the top panels show the kinematic front. Calculations show that, after some time, the lens will cross this front, as also shown in the schematic diagram in Richardson and Tychensky (1998). As in the oceanic observations, the northward meander of the jet above the ITL initially, decreases in amplitude and the jet straightens up as the ITL crosses it. Also, a cyclonic meander grows in the upper layer, east of the ITL, and couples with it, leading to a southward displacement of this two-layer vortex dipole.

4. The main results

These numerical experiments, despite their simplicity, describe and characterise various interactions between different intrathermocline vortices and a surface jet/front (Rossby *et al.* 1988, Richardson *et al.* 1989, Hogg and Stommel 1990). It must be underlined that these experiments describe essentially the first stage of this interaction since no mechanism of jet restoration towards a zonal state is included here (no beta effect, no wind forcing, no relaxation towards a large scale meridional density gradient). Therefore, the meanders amplitude in our model are not constrained in their growth.

The various experiments showed that

(1) the jet has a critical effect on the lens motion, changing their velocity and direction; it tends to (temporarily) slow down their zonal propagation and accelerate its meridional propagation via the formation of large meanders; it is a barrier for the propagation of vortices like-signed with the gyre they are initially embedded in, but can be crossed by opposite-signed vortices (Vandermeirsch *et al.* 2003a,b);
(2) ITLs can have a strong effect on the jet, considerably changing its topological properties; the jet deformation grows with time and smaller wavelength components of the perturbation develop, corresponding to thin and long meanders. Such meanders circle the ITL that crossed the front. This can be an indirect means of detecting ITLs crossing surface fronts. Also, the coupling of a cyclonic filament with an anticyclonic ITL south of the front will lead to the southward advection of this baroclinic dipole;
(3) ITL merger under, or below and near, a surface front is possible. Merger north of, or under the jet axis, will lead to much deformation of the middle layer vortex. ITL merger south of the front will allow the production of small vortices in the middle layer which do not disappear within 3 months time;
(4) the interaction of an ITL dipole with a surface front leads to different outcomes depending on the initial orientation of the dipole propagation. Eastward or southeastward propagating dipoles usually follow the jet axis finally. Southward and southwestward dipoles split up : the deep cyclone pairs with a cyclonic meander of the jet but does not cross the front. The deep anticyclone crosses the front and pairs with another surface cyclone, thus creating a baroclinic dipole which propagates southward;
(5) intrathermocline vortices with radii close to the first baroclinic radius of deformation remain quite stable during the crossing of the jet. They sometimes become

slightly elliptical in the shear created by the surface jet, but they do not break up. Therefore, ITL growth is favoured against ITL decay in our experiments.

Nevertheless, as stated above, these experiments remain quite simple compared with the complex oceanic reality. No beta effect, no large scale density gradients nor wind forcing are included here so that the jet is not restored towards its zonal position. No surface turbulence is included so that the ITLs do not couple with other surface vortices than those created by the jet deformation, in the course of these experiments. No topographic feature is included with which the ITLs could interact and possibly decay.

Also the simple three-layer model does not allow a vertical deformation of the ITLs during jet crossing. This could be studied in a five-layer model, or in a model with continuous vertical stratification. Finally, the use of a quasi-geostrophic model prevents the development of strong ageostrophic motions which are associated with submesoscale motions. The study of surface jet – ITL interaction in a primitive equation model would thus be of interest to evaluate the formation and survival rate of small eddies during this process.

Acknowledgements

The authors wish to thank the editors, Pr. David Dritschel and Pr. Andrew Soward, for their help and for efficient handling of this paper.

Disclosure statement

No potential conflict of interest was reported by the authors.

Funding

The work was performed in the frame of Russian-French project PRS [grant number 16-55-15001] from RFBR/CNRS (applications to ocean). MAS, BNF and OIY were supported also by [grant number 14-50-00095] from RSF (numerical simulation).

References

Aguiar, A.C.B., Peliz, A. and Carton, X., A census of meddies in a long-term high-resolution simulation. *Prog. Oceanogr.* 2013, **116**, 80–94.

Aleynik, D.L., Plakhin, E.A. and Filyushkin, B.N., On the mechanism of formation of intrathermocline lenses in the canyon area of the Gulf of Cadiz continental slope. *Oceanology* 1998, **38**, 645–653.

Alvez, J.M.R., Carton, X. and Ambar, I., Hydrological structure, circulation and water mass transport in the gulf of Cadiz. *Int. J. Geosci.* 2011, **2**, 432–456.

Ambar, I., A shallow core of Mediterranean water off western Portugal. *Deep-Sea Res. Part A* 1983, **30**, 677–680.

Andrade, I., Hormazábal, S. and Combes, V., Intrathermocline eddies at the Juan Fernández Archipelago, southeastern Pacific Ocean. *Lat. Am. J. Aquat. Res.* 2014, **42**, 888–906.

Antkowiak, A. and Brancher, P., Transient energy growth for the Lamb-Oseen vortex. *Phys. Fluids* 2004, **16**, L1–L4. doi:10.1063/1.1626123.

Armi, L., Hebert, D., Oakey, N., Price, J.F., Richardson, P.L., Rossby, H.T. and Ruddick, B., Two year in the life of a Mediterranean salt lens. *J. Phys. Oceanogr.* 1989, **19**, 354–370.

Armi, L. and Stommel, H., Four views of a portion of the North Atlantic subtropical gyre. *J. Phys. Oceanogr.* 1983, **13**, 828–857.
Armi, L. and Zenk, W., Large lenses of highly saline Mediterranean water. *J. Phys. Oceanogr.* 1984, **14**, 1560–1576.
Baird, M.E. and Ridgway, K.R., The southward transport of sub-mesoscale lenses of Bass Strait Water in the centre of anti-cyclonic mesoscale eddies. *Geophys. Res. Lett.* 2012, **39**, L05603. doi:10.1029/2011GL050643.
Bashmachnikov, I. and Carton, X., Surface signature of Mediterranean water eddies in the Northeastern Atlantic: effect of the upper ocean stratification. *Ocean Sci.* 2012, **8**, 931–943.
Bashmachnikov, I., Carton, X. and Belonenko, T.V., Characteristics of surface signatures of Mediterranean water eddies. *J. Geophys. Res. Oceans* 2014, **119**. doi:10.1002/2014JC010244.
Bashmachnikov, I., Neves, F., Calheiros, T. and Carton, X., Properties and pathways of Mediterranean water eddies in the Atlantic. *Progr. Oceanogr. Part A* 2015, **137**, 149–172.
Belkin, I.M., Emelyanov, M.V., Kostyanoy, A.G. and Fedorov, K.N., Thermohaline structure of intermediate waters of the ocean and intrathermocline eddies. In *Intrathermocline Eddies in the Ocean*, edited by K.N. Fedorov, pp. 8–34, 1986 (P.P. Shirshov Institute of Oceanology: Moscow).
Bower, A.S. and Furey, H.H., Mesoscale eddies in the Gulf of Aden and their impact on the spreading of Red Sea Outflow Water. *Progr. Oceanogr.* 2012, **96**, 14–39.
Bower, A.S., Serra, N. and Ambar, I., Structure of the Mediterranean undercurrent and Mediterranean water spreading around the southwestern Iberian Peninsula. *J. Geophys. Res.* 2002, **107**, 3161. doi:10.1029/2001JC001007.
Brundage, W.L. and Dugan, J.P., Observations of an anticyclonic eddy of 18°C water in the Sargasso Sea. *J. Phys. Oceanogr.* 1986, **16**, 717–727.
Carton, X., Chérubin, L., Paillet, J., Morel, Y., Serpette, A. and Le Cann, B., Meddy coupling with a deep cyclone in the Gulf of Cadiz. *J. Mar. Syst.* 2002, **32**, 13–42.
Carton, X., Daniault, N., Alves, J., Cherubin, L. and Ambar, I., Meddy dynamics and interaction with neighboring eddies southwest of Portugal: observations and modeling. *J. Geophys. Res. Oceans* 2010, **115**. doi:10.1029/2009JC005646.
Ciani, D., Carton, X., Bashmachnikov, I. and Chapron, B., Influence of deep vortices on the ocean surface. *Nonlin. Discont. Complex.* 2015, **4**, 281–312.
Dritschel, D.G., Contour surgery: a topological reconnection scheme for extended integrations using contour dynamics. *J. Comput. Phys.* 1988, **77**, 240–266.
Dugan, J.P., Mied, R.P., Mignerey, P.C. and Schuetz, A.F., Compact, intrathermocline eddies in the Sargasso Sea. *J. Geophys. Res. Oceans* 1982, **87**, 385–393.
Fedorov, K.N. and Ginzburg, A.I., Mushroom-like currents (vortex dipoles): one of the most widespread forms of non-stationary coherent motions in the ocean. In *Mesoscale/Synoptic Coherent structures in Geophysical Turbulence*, Elsevier Oceanography Series, edited by J.C.J. Nihoul, B.M. Jamaat, pp. 1–14, 1989 (Elsevier: Amsterdam/Oxford/New York/Tokyo).
Fedorov, K.N. and Meshchanov, S.L., Structure and propagation of Red Sea waters in the Gulf of Aden. *Oceanology* 1988, **28**, 279–284.
Filyushkin, B.N., Investigation of intrathermocline lenses of Mediterranean origin (Cruise 16 of R/V "Vityaz", June 3 – September 16, 1988. *Oceanology* 1989, **29**, 535–536.
Filyushkin, B.N., Aleynik, D.L., Kozhelupova, N.G. and Moshonkin, S.N., Horizontal transport peculiarities of the Mediterranean water in the Atlantic. In *Ocean and Sea Research*, edited by V.F. Komchatov, Vol. 212, Proceedings State Oceanography Institute, pp. 76–88, 2009. (Moscow).
Filyushkin, B.N. and Plakhin, E.A., Experimental study of the first stage of Mediterranean water lens formation. *Oceanology* 1996, **35**, 797–804.
Filyushkin, B.N. and Sokolovskiy, M.A., Modeling the evolution of intrathermocline lenses in the Atlantic Ocean. *J. Mar. Res.* 2011, **69**, 191–220.
Filyushkin, B.N., Sokolovskiy, M.A., Kozhelupova, N.G. and Vagina, I.M., Dynamics of intrathermocline lenses. *Dokl. Earth Sci.* 2010, **434**, 1377–1380.
Filyushkin, B.N., Sokolovskiy, M.A., Kozhelupova, N.G. and Vagina, I.M., Reflection of intrathermocline eddies on the ocean surface. *Dokl. Earth Sci.* 2011, **439**, 986–989.

Filyushkin, B.N., Sokolovskiy, M.A., Kozhelupova, N.G. and Vagina, I.M., Lagrangian methods for observation of intrathermocline eddies in ocean. *Oceanology* 2014, **54**, 688–694.
Gordon, A.L., Giulivi, C.F., Lee, C.M., Furey, H.H., Bower, A. and Talley, L., Japan/East Sea intrathermocline eddies. *J. Phys. Oceanogr.* 2002, **32**, 1962–1974.
Hogan, P.J. and Hurlburt, H.E., Why do intrathermocline eddies form in the Japan/East Sea? *A modeling perspective. Oceanography* 2006, **66**, 134–143.
Hogg, N.G. and Stommel, H.M., How currents in upper thermocline could advect meddies deeper down. *Deep Sea Res. Part A* 1990, **37**, 613–623.
Hunkins, K.L., Subsurface eddies in the Arctic Ocean. *Deep Sea Res.* 1974, **21**, 1017–1033.
Ivanov, Y.A. and Filyushkin, Y.B., Experimental investigation in the Azores current frontal zone. *Oceanology* 1995, **35**, 169–175.
Ivanov, Y.A., Kort, V.G., Shapovalov, S.M. and Sherbinin, A.D., Mesoscale intrusion lenses. In *Proceedings Hydrophysical Studies at Mesopolygon Program*, pp. 41–46, 1998 (Science: Moscow), in Russian.
Johnson, J.L., Ambar, I., Serra, N. and Stevens, I., Comparative studies of the spreading of Mediterranean water through the Culf Cádiz. *Deep-Sea Res. Part II* 2002, **49**, 4179–4193.
Käse, R.H. and Siedler, G., Meandering of the subtropical front southeast of Azores. *Nature* 1982, **300**, 245–246.
Käse, R.H. and Zenk, W., Reconstructed Mediterranean salt lens trajectories. *J. Phys. Oceanogr.* 1987, **17**, 158–161.
Käse, R.H. and Zenk, W., Structure of the Mediterranean Water and meddy characteristics in the Northeastern Atlantic. In *The Warmwatersphere of the North Atlantic Ocean*, edited by W. Krauss, pp. 365–395, 1996 (Gebrüder Borntraeger: Stuttgart, Berlin).
Kizner, Z. and Khvoles, R., Two variations on the theme of Lamb-Cchaplygin: supersmooth dipole and rotating multipoles. *Reg. Chaot. Dyn.* 2004, **9**, 509–518.
Kostianoy, A.G. and Belkin, G.M., A survey of observations on intrathermocline eddies in the world ocean. In *Mesoscale/Synoptic Coherent structures in Geophysical Turbulence*, Elsevier Oceanography Series, edited by J.C.J. Nihoul and B.M. Jamaat, pp. 821–841, 1989 (Elsevier: Amsterdam/Oxford/New York/Tokyo).
Kozlov, V.F. and Sal'nikov, P.Y., Mechanism for the formation of mushroom-shaped flows with dense packing of vortices. *Izvestiya, Atmos. Ocean. Phys.* 1989, **25**, 324–326.
Lamb, H., *Hydrodynamics*, 6th ed., 241 p, 1932 (Cambridge: Cambridge University Press).
Lebedev, K.V., An Argo-based model for investigation of the global ocean physics (AMIGO). *Oceanology*, 2016, submitted.
L'Hégaret, P., Carton, X., Ambar, I., Ménesguen, C., Hua, B.L., Chérubin, L., Aguiar, A., Le Cann, B., Daniault, N. and Serra, N., Evidence of Mediterranean Water dipole collision in the Gulf of Cádiz. *J. Geophys. Res. Oceans* 2014, **119**, 5337–5359.
L'Hégaret, P., Duarte, R., Carton, X., Vic, C., Ciani, D., Baraille, R. and Corréard, S., Seasonal mesoscale variability in the Arabian Sea from HYCOM model and observations: impact on the Persian Gulf Water path. *Ocean Sci.* 2015, **11**, 667–693.
Lilly, J.M. and Rhines, P.B., Coherent eddies in the Labrador Sea observed from a mooring. *J. Phys. Oceanogr.* 2002, **32**, 585–598.
Madelain, F., Influence de la topographie du fond sur lécoulement Méditerranen entre le Détroit de Gibralter et le cap Saint-Vincent. *Cahiers Oceanogr.* 1970, **XII annee. N 1**, 43–62.
Makarov, V.G., Computational algorithm of the contour dynamics method with changeable topology of domains under study. *Model. Mekh.* 1991, **5**, 83–95.
Martin, A.P., Wade, I.P., Richards, K.J. and Heywood, K.J., The PRIME eddy. *J. Mar. Res.* 1998, **56**, 439–462.
Maximenko, N. and Yamagata, T., Submesoscale anomalies in the North Pacific Subarctic front. *J. Geophys. Res. Oceans* 1995, **100**, 18459–18469.
McDowell, S.E. and Rossby, H.T., Mediterranean water: An intense mesoscale eddy off the Bahamas. *Science* 1978, **202**, 1085–1087.
Meschanov, S.L. and Shapiro, G.I., A young lens of Red Sea water in the Arabian Sea. *Deep Sea Res. Part* 1998, **I**(45), 1–13.

Paillet, J., Le Cann, B., Carton, X., Morel, Y. and Serpette, A., Dynamics and evolution of a northern Meddy. *J. Phys Oceanogr.* 2002, **32**, 55–79.
Pelland, N.A., Eriksen, C.C. and Lee, C.M., Subthermocline eddies over the Washington continental slope as observed by seagliders, 2003–09. *J. Phys. Oceanogr.* 2013, **43**, 1026–1053.
Pingree, R.D., The droguing of Meddy Pinball and seeding with ALACE floats. *J. Mar. Biol. Assoc. U. K.* 1995, **75**, 235–252.
Pingree, R.D. and Le Cann, B., Structure of a meddy (Bobby 92) southeast of the Azores. *Deep Sea Res. Part I* 1993a, **40**, 2077–2103.
Pingree, R.D. and Le Cann, B., A shallow meddy (a Smeddy) from the secondary Mediterranean salinity maximum. *J. Geophys. Res. Oceans* 1993b, **98**, 20169–20185.
Prants, S.V., Budyansky, M.V. and Uleysky, MYu, Identifying Lagrangian fronts with favourable fishery conditions. *Deep Sea Res. Part I* 2014, **90**, 27–35.
Prater, M.D. and Rossby, T., An alternative hypothesis for the origin of the "Mediterranean" salt lens observed off the Bahamas in the fall of 1976. *J. Phys. Oceanogr.* 1999, **29**, 2103–2109.
Prater, M.D. and Sanford, T.B., A meddy off Cape St. Vincent. Part 1: Description. *J. Phys. Oceanogr.* 1994, **24**, 15–86.
Richardson, P.L., Bower, A.S. and Zenk, Z., A census of meddies tracked by floats. *Progr. Oceanogr.* 2000, **45**, 209–250.
Richardson, P.L., McCartney, M.S. and Maillard, C., A search for meddies in historical data. *Dyn. Atmos. Oceans* 1991, **15**, 241–265.
Richardson, P.L. and Tychensky, A., Meddy trajectories in the Canary Basin measured during the SEMAPHORE experiment, 1993–1995. *J. Geophys Res.* 1998, **103**, 25029–25045.
Richardson, P.L., Walsh, D., Armi, L., Schröder, M. and Price, J.F., Tracking three meddies with SOFAR floats. *J. Phys. Oceanogr.* 1989, **19**, 371–383.
Rossby, T., Five drifters in a Mediterranean salt lens. *Deep Sea Res. Part A* 1988, **35**, 1653–1663.
Sadoux, S., Baey, J., Fincham, A. and Renouard, D., Experimental study of the stability of an intermediate current and its interaction with a cape. *Dyn. Atmos. Oceans* 2000, **31**, 165–192.
Tokos, Schultz, K., Hinrichsen, H. H. and Zenk, W., Merging and migration of two meddies. *J. Phys. Oceanogr.* 1994, **24**, 2129–2141.
Serra, N. and Ambar, I., Eddy generation in the Mediterranean undercurrent. *Deep-Sea Res. Part* 2002, **II**(49), 4225–4243.
Serra, N., Ambar, I. and Boutov, D., Surface expression of Mediterranean Water dipoles and their contribution to the shelf/slope open ocean exchange. *Ocean Sci.* 2010, **6**, 191–209. Available online at: http://www.ocean-sci.net/6/191/2010/.
Serra, N., Ambar, I. and Käse, R.H., Observations and numerical modelling of the Mediterranean outflow splitting and eddy generation. *Deep-Sea Res. Part II* 2005, **52**, 383–408.
Sokolovskiy, M.A., Modeling triple-layer vortical motions in the ocean by the contour dynamics method. *Izvestiya, Atmos. Ocean. Phys.* 1991, **27**, 380–388.
Sokolovskiy, M.A., Stability of an axisymmetric three-layer vortex. *Izvestiya, Atmos. Ocean. Phys.* 1997, **33**, 16–26.
Sokolovskiy, M.A., Stability analysis of the axisymmetric three-layered vortex using contour dynamics method. *Comput. Fluid Dyn. J.* 1997, **6**, 133–156.
Sokolovskiy, M.A. and Filyushkin, B.N., Interaction between synoptic gyres and intrathermocline lenses. *Oceanology* 2015, **55**, 661–666.
Sokolovskiy, M.A., Filyushkin, B.N. and Carton, X.J., Dynamics of intrathermocline vortices in a gyre flow over a seamount chain. *Ocean Dyn.* 2013, **63**, 741–760.
Sokolovskiy, M.A. and Verron, J., *Dynamics of vortex structures in a stratified rotating fluid*, Atmospheric and Oceanographic Sciences Library, Vol. 47, 382 p, 2014 (Springer: Cham/Heidelberg/New York/Dordrecht/London).
Stammer, D., On eddy characteristics, eddy transports, and mean flow properties. *J. Phys. Oceanogr.* 1998, **28**, 727–739.
Stammer, D., Hinrichsen, H.H. and Käse, R.H., Can meddies be detected by satellite altimetry? *J. Geophys. Res. Oceans* 1991, **96**, 7005–7014.

Thorpe, S.A., Turbulence in the stratified and rotating world ocean. *Theor. Comput. Fluid Dyn.* 1998, **11**, 171–181.
Tychensky, A. and Carton, X., Hydrological and dynamical characterization of meddies in the Azores region: a paradigm for baroclinic vortex dynamics. *J. Geophys. Res.* 1998, **103**, 25061–25079.
Vandermeirsch, F.O., Carton, X.J. and Morel, Y.G., Interaction between an eddy and a zonal jet. Part I. One and a half layer model. *Dyn. Atmos. Oceans* 2003, **36**, 247–270.
Vandermeirsch, F.O., Carton, X.J. and Morel, Y.G., Interaction between an eddy and a zonal jet. Part II. Two and a half layer model. *Dyn. Atmos. Oceans* 2003, **36**, 271–296.
Vic, C., Roullet, G., Capet, X., Carton, X., Molemaker, M.J. and Gula, J., Eddy-topography interactions and the fate of the Persian Gulf Outflow. *J. Geophys. Res.* 2015, **120**, 6700–6717.
Zhou, M., Paduan, J.D. and Niiler, P.P., Surface currents in the Canary Basin from drifter observations. *J. Geophys. Res.* 2000, **105**, 21893–21911.